Structural, transport, magnetic properties and Raman spectroscopy of orthorhombic $Y_{1-x}Ca_xMnO_3$ ($0 \leq x \leq 0.5$)

2005 J. Phys.: Condens. Matter 17 3333

(http://iopscience.iop.org/0953-8984/17/21/026)

INSTITUTE OF PHYSICS PUBLISHING JOURNAL OF PHYSICS: CONDENSED MATTER

J. Phys.: Condens. Matter **17** (2005) 3333–3341 doi:10.1088/0953-8984/17/21/026

Structural, transport, magnetic properties and Raman spectroscopy of orthorhombic $Y_{1-x}Ca_xMnO_3$ ($0 \leqslant x \leqslant 0.5$)

M N Iliev[1,4], B Lorenz[1], A P Litvinchuk[1], Y-Q Wang[1], Y Y Sun[1] and C W Chu[1,2,3]

[1] Texas Center for Superconductivity and Advanced Materials, and Department of Physics, University of Houston, Houston, TX 77204-5002, USA
[2] Lawrence Berkeley National Laboratory, One Cyclotron Road, Berkeley, CA 94720, USA
[3] Hong Kong University of Science and Technology, Hong Kong, People's Republic of China

E-mail: miliev@uh.edu

Received 4 November 2004, in final form 17 February 2005
Published 13 May 2005
Online at stacks.iop.org/JPhysCM/17/3333

Abstract

Orthorhombic $Y_{1-x}Ca_xMnO_3$ ($0 \leqslant x \leqslant 0.5$) was prepared, and the variations with x of its structural, magnetic, and electrical properties and the polarized Raman spectra were investigated. The lattice parameters change systematically with x. Although there are strong indications for increasing disorder above $x = 0.20$, the average structure remains orthorhombic in the whole substitutional range. Ca doping increases the conductivity, but the temperature dependence of resistivity $\rho(T)$ remains semiconducting for all x. The average magnetic exchange interaction changes from antiferromagnetic for $x < 0.08$ to ferromagnetic for $x > 0.08$. The evolution with x of the Raman spectra provides evidence for an increasingly disordered oxygen sublattice at $x \geqslant 0.10$, presumably due to quasistatic and/or dynamical Jahn–Teller distortions.

1. Introduction

At atmospheric pressure, $Y_{1-x}Ca_xMnO_3$ ($0 \leqslant x < 0.25$), similar to the rare-earth manganites $RMnO_3$, for R with smaller ionic radius (R = Ho, Er, Tm, Yb, Lu), crystallizes in the hexagonal $P6_3cm$ structure, whereas the orthorhombic, distorted perovskite structure is the stable phase for $Y_{1-x}Ca_xMnO_3$ with $x \geqslant 0.25$ [1]. Upon annealing under high pressure, some hexagonal manganites, such as $YMnO_3$ and $HoMnO_3$, can be converted to their orthorhombic $Pnma$ phase [2]. The Ca- and Sr-doped orthorhombic rare-earth manganites have been a subject of intensive studies since the phenomenon 'colossal magnetoresistance' (CMR)

[4] Author to whom any correspondence should be addressed.

has been rediscovered [3]. To our knowledge, there are, however, no reports on the synthesis and properties of doped yttrium-based orthorhombic manganites for $x < 0.25$. The $Y_{1-x}Ca_xMnO_3$ orthorhombic system is of particular interest as it could be compared to the model $La_{1-x}Ca_xMnO_3$ system, where Ca doping and conversion of part of the Jahn–Teller Mn^{3+} ions to non-Jahn–Teller Mn^{4+} ions results in a complex magnetic phase diagram and strong interplay between structural, magnetic, and transport properties.

In this work we report the synthesis of the orthorhombic series $Y_{1-x}Ca_xMnO_3$ and the first results on the variations with x of structural parameters, resistivity, magnetic properties, and Raman spectra over the doping range $0 \leqslant x \leqslant 0.5$.

2. Samples and experimental details

As a first step in sample preparation, ceramic pellets of hexagonal $Y_{1-x}Ca_xMnO_3$ ($x = 0.00$, 0.03, 0.06, 0.10, and 0.20) and orthorhombic $Y_{1-x}Ca_xMnO_3$ ($x = 0.30$ and 0.50) were synthesized by solid state reaction. The prescribed amounts of Y_2O_3, $CaCO_3$, and Mn_2O_3 were mixed and preheated at 900–1000 °C in oxygen for 16 h followed by sintering at 1140–1170 °C for 24 h under oxygen atmosphere. The hexagonal samples were resintered in a high-pressure furnace under 35 kbar at 1015–1030 °C for 5 h. Under these conditions the hexagonal phase was completely transformed into the metastable orthorhombic structure. The x-ray diffraction (XRD) patterns were collected at room temperature using a Rigaku DMaxIII/B x-ray diffractometer.

Magnetization measurements were conducted employing an MPMS SQUID magnetometer (Quantum Design) at an external field of 500 Oe. The dc resistivity was measured by the standard four-probe method using a Keithley 220 current source and a Keithley 182 nanovoltmeter. The Raman spectra were obtained at room temperature using an HR640 spectrometer equipped with a microscope, notch filters, and a liquid-nitrogen-cooled CCD detector. 514.5 and 632.8 nm laser lines, focused with a 100× objective on the sample's surface in a spot of (2–3 μm) diameter, were used for excitation. For most samples, the size of the microcrystals constituting the pellet was larger than the laser spot, which made it possible to select microcrystals with proper orientation of crystallographic axes with respect to the incident polarization and obtain polarized spectra in nearly exact scattering configurations.

3. Results and discussion

3.1. Structural, electric, and magnetic measurements

The x-ray spectra of $Y_{1-x}Ca_xMnO_3$ are shown in figure 1 for $x = 0$–0.5. All reflections can be indexed within the orthorhombic symmetry, space group *Pnma*. The absence of impurity lines proves the high phase purity and the success of the high-pressure synthesis in stabilizing the *Pnma* structure for Ca content between 0 and 0.5. A substantial broadening of the x-ray lines is observed above $x = 0.2$, indicating an increased disorder at higher substitution, x. The lattice constants change systematically with x, as shown in figure 2. The largest change is the decrease of a by up to 7% at $x = 0.5$. In contrast, the c-axis is almost completely unaffected by the Ca doping. The b-axis shows a distinct, but moderate, increase from $x = 0$ to 0.5, the total change being no more than 1.5%. The systematic change of the lattice constants with x and the absence of impurity lines in the x-ray spectra unambiguously prove that the Ca ions in fact replace the Y ions in the perovskite-like structure of $Y_{1-x}Ca_xMnO_3$. Our values of the lattice parameters are in good agreement with data of recent publications for $x = 0$, 0.25, 0.3, and 0.5 (included in figure 2 using symbols listed in the legend) [4–7]. Recent neutron

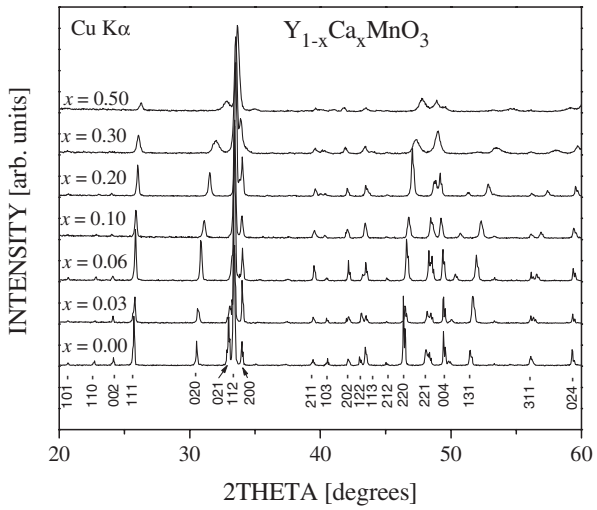

Figure 1. X-ray diffraction pattern of $Y_{1-x}Ca_xMnO_3$ ($0 \leqslant x \leqslant 0.5$).

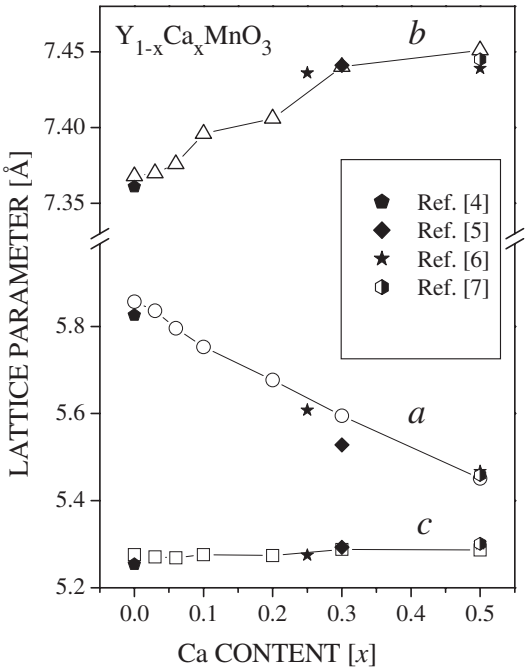

Figure 2. Variation of the lattice parameters of $Y_{1-x}Ca_xMnO_3$ with x.

powder diffraction (NPD) experiments [8] estimated a considerably longer a-axis (5.97 Å as compared with the 5.857 Å of the present investigation). The discrepancy is probably due to the excess oxygen reported for the NPD samples.

The doping of orthorhombic $YMnO_3$ with Ca introduces charge carriers by removing one electron per Ca from the Mn^{3+} ions. The resulting Mn^{4+} 'carries' one hole that can hop among the Mn ions via the hybridization of Mn d-states with the O p-states. The conductivity of the

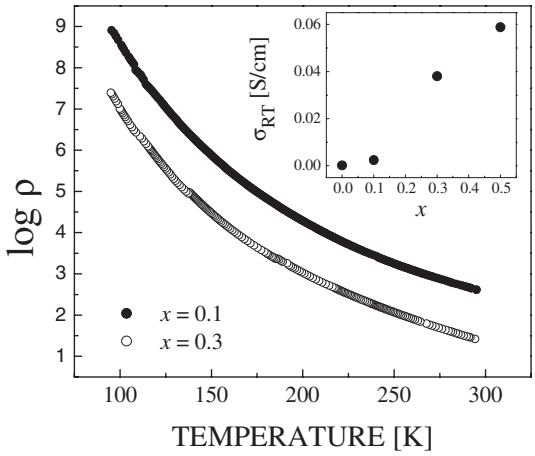

Figure 3. Resistivity of $Y_{1-x}Ca_xMnO_3$ as a function of temperature (for $x = 0.1$ and 0.3). Inset: room-temperature conductivity as a function of x.

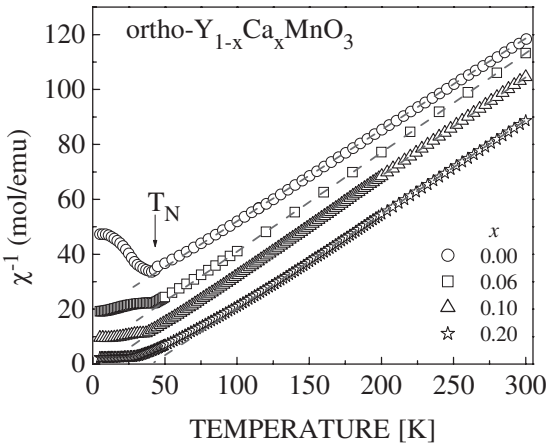

Figure 4. Inverse magnetic susceptibility of orthorhombic $Y_{1-x}Ca_xMnO_3$ for $x = 0$–0.2.

doped compound should increase with x. In fact, the room-temperature conductivity of ortho-$YMnO_3$ increases by a factor of about 300 between $x = 0$ and 0.5 (see the inset of figure 3). The characteristic temperature dependence of the resistivity, $\rho(T)$, is semiconducting for all $x < 0.5$. Figure 3 (main panel) shows two typical examples of $\rho(T)$ for $x = 0.1$ and 0.3.

The magnetic properties of the series $Y_{1-x}Ca_xMnO_3$ are summarized in figure 4. For $x = 0$ the inverse magnetic susceptibility exhibits a Curie–Weiss-like linear temperature dependence at $T > 80$ K and a sharp anomaly at the antiferromagnetic transition temperature, $T_N = 42.5$ K. From the high-temperature data the paramagnetic Curie temperature and the effective magnetic moment per Mn ion are estimated as $\Theta = -54.7$ K and $\mu_{eff} = 5.05\ \mu_B$, respectively. The effective moment is close to the value of 4.9 μ_B for the free Mn^{3+} ion (spin only, $S = 2$). The values for Θ and μ_{eff} are in good agreement with those reported in [9] (-67 K, 4.98 μ_B), but deviate significantly from recent results (-26 K, 3.69 μ_B) of [8]. We attribute the latter discrepancy to the presence of a significant amount of hexagonal $YMnO_3$ and excess oxygen in the samples of [8]. The high-pressure-synthesized specimens used in the

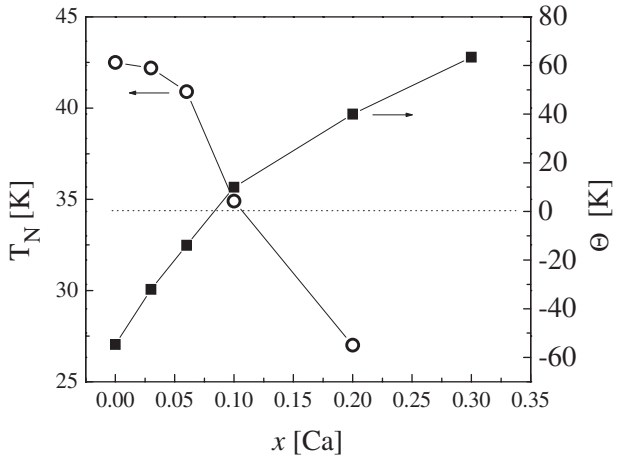

Figure 5. Effective paramagnetic Curie temperature of orthorhombic $Y_{1-x}Ca_xMnO_3$ estimated from the high-temperature magnetic susceptibility (filled squares, right scale) and the Néel temperature for the AFM transition (open circles, left scale).

present investigation are of high phase purity. The clear decrease of the magnetic susceptibility below T_N is a further indication that the composition of the compound is close to stoichiometric. Deviations from stoichiometry (e.g. excess oxygen) will result in the presence of Mn^{4+} ions with a paramagnetic contribution to the susceptibility that can easily be detected below T_N.

The doping of ortho-$YMnO_3$ with Ca^{2+} results in a change of magnetic properties. Up to $x = 0.3$, the high-temperature susceptibility still exhibits Curie–Weiss behaviour (figure 4). With increasing x the effective moment changes very little but Θ increases rapidly from -55 K ($x = 0$) to +63 K at $x = 0.3$. Figure 5 shows Θ as a function of x. The paramagnetic Curie temperature crosses zero at close to 8% of Ca doping. The change of sign of Θ indicates a change of the average magnetic exchange interaction from antiferromagnetic (AFM, $x < 0.08$) to ferromagnetic (FM, $x > 0.08$), as illustrated in figure 5. This change is a consequence of the presence of Mn^{4+} ions for $x > 0$. For $x = 0$, the magnetic exchange of two neighbouring Mn^{3+} is mediated by the oxygen ions between them and is ascribed to the superexchange mechanism with a resulting AFM coupling of the moments. With Ca doping Mn^{4+} ions are created. These Mn^{4+} ions do not participate in the superexchange interaction but open the double exchange interaction channel whenever they are next to an Mn^{3+}. The double exchange is ferromagnetic in its nature because of a gain in kinetic energy (the hole at the Mn^{4+} can hop to the neighbouring Mn^{3+}) if the magnetic moments of both Mn ions are parallel. This explains the gradual crossover of the paramagnetic Curie temperature from negative to positive values with increasing x as estimated from the high-T susceptibility data. Note that Θ obtained from the data shown in figure 5 is an effective quantity, characteristic for the average response to field and temperature of all Mn moments, those coupled by AFM superexchange as well as those coupled by FM double exchange interactions to their respective neighbours. Our data clearly demonstrate that Ca doping of orthorhombic $YMnO_3$ is a powerful tool to tune the spin correlations from AFM superexchange to predominantly FM double exchange correlations. However, the increasing FM spin coupling does not introduce ferromagnetic long-range order down to the lowest temperatures in agreement with recent results for $x = 0.3$ [6]. The low-temperature AFM Néel transition of *ortho*-$YMnO_3$ is also affected by the Ca doping. The relative enhancement of the magnetic susceptibility below T_N for $x > 0$ (as compared to

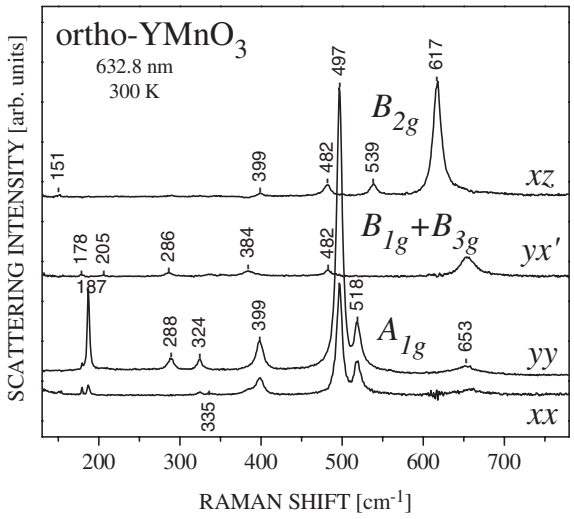

Figure 6. Polarized Raman spectra of $YMnO_3$. The assignment of Raman lines to particular atomic motions is given in [10].

$x = 0$) is an indication of the presence of Mn^{4+} ions and their paramagnetic contribution to the spin susceptibility. The Néel temperature decreases with increasing x due to a gradual reduction of the AFM superexchange correlations (figure 5). The AFM transition is sharp up to $x = 0.2$, but it broadens at higher doping levels. Only data for T_N up to $x = 0.2$ have therefore been included in the figure. The broadening of the magnetic transition above $x = 0.2$ is consistent with the observed broadening of the x-ray reflections and the Raman bands (see the next section) and with the model of short-range ferromagnetism and a spin glass state proposed recently for $x = 0.3$ [6]. It indicates the increasing influence of disorder on the physical properties of ortho-$Y_{1-x}Ca_xMnO_3$.

3.2. Raman spectra

The polarized Raman spectra of undoped $YMnO_3$, shown in figure 6, are identical to those reported in [10], where an assignment of the lines to particular phonon modes has also been done. The variations with x of the spectra of $Y_{1-x}Ca_xMnO_3$, measured with parallel (HH) and crossed (HV) scattering configurations, are shown in figure 7. The HH configuration is close to xx and the Raman lines correspond to modes of A_g symmetry. The modes allowed with the HV (nearly xz) configuration are of B_{2g} symmetry.

As it follows from figure 7, within the doping range $0 \leqslant x \leqslant 0.10$ the line widths moderately increase with x, but their position and relative intensity remain practically unchanged. At $x = 0.10$ there is a visible increase in intensity of the high-frequency HH band at 644 cm^{-1} and the HV band at 654 cm^{-1}. For $x = 0.20$ these bands broaden, increase further in intensity, and shift towards lower wavenumbers along with the bands originating from the 496 cm^{-1} (A_g) and 617 cm^{-1} (B_{2g}) lines. At $x = 0.30$ the overall intensities of the spectra are reduced. The HV spectrum consists of only two broad bands centred at 495 and 624 cm^{-1}. In addition to broad bands close to these positions, the corresponding HH spectrum contains two weak bands at lower wavenumbers. The evolution of the HV spectrum between $x = 0.10$ and 0.30 is given in more detail in figure 8. No Raman bands of detectable intensity are observed for $x = 0.5$.

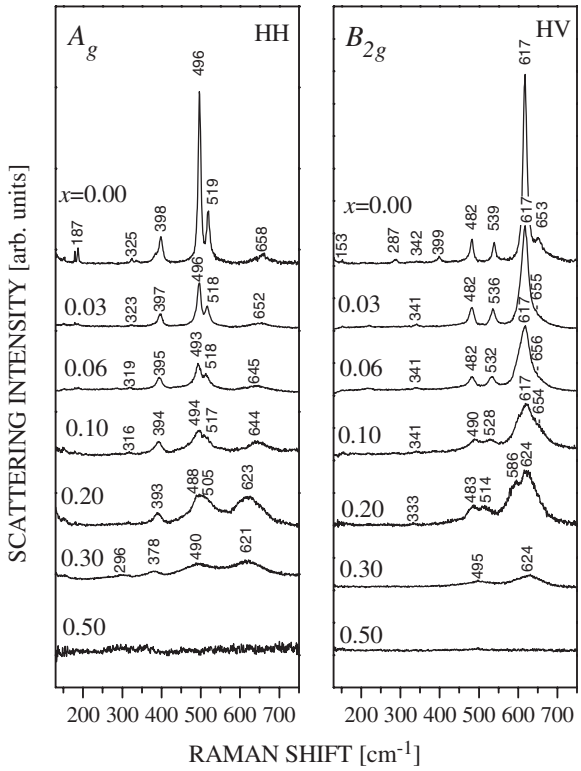

Figure 7. Variations with x of the Raman spectra of $Y_{1-x}Ca_xMnO_3$. The HH and HV configurations are close to xx and xz, respectively.

The Raman spectra for $x \geqslant 0.10$ are similar to those reported earlier for other $R^{3+}_{1-x}A^{2+}_xMnO_3$ (R = rare earth, A = Ca, Sr, Ba; $x \geqslant 0.1$) systems [11–17], where two or three broad bands are observed at positions close to those of the strongest lines for nominally undoped $RMnO_3$. On the basis of this closeness, the broad bands have usually been assigned to the corresponding Raman-allowed modes in the parent *Pnma* structure.

An alternative explanation for the broad band origin has recently been proposed by Iliev *et al* [18]. It has been argued that at higher doping levels the spectral profiles reflect a smeared partial phonon density-of-states (PDOS) related to oxygen vibrations rather than broadened Γ-point Raman-allowed phonon modes. Indeed, the coexistence in doped manganites of Jahn–Teller-distorted ($Mn^{3+}O_6$) and undistorted ($Mn^{4+}O_6$) octahedra and the $Mn^{3+} \leftrightarrow Mn^{4+}$ charge transfer results in strong quasistatic and/or dynamical Jahn–Teller disorder of the oxygen sublattice. The loss of translational symmetry activates otherwise Raman-forbidden oxygen vibrations, corresponding to the off-centre phonon modes in the ordered parent compound. In support of this model are: (i) the good correspondence between experimental Raman profiles and the calculated smeared PDOS; (ii) the consistent explanation of the similarities between the Raman spectra of manganites with different average structures (orthorhombic or rhombohedral); and (iii) the strong reduction or disappearance of the broad bands below the insulator-to-metal transition in the CMR materials.

Our results support the assumption of the dominant role of Jahn–Teller-disorder-induced bands in the Raman spectra of heavily doped orthorhombic manganites. Indeed, the Raman spectrum of undoped $YMnO_3$ is well understood and the A_g line at 519 cm^{-1} and the B_{2g}

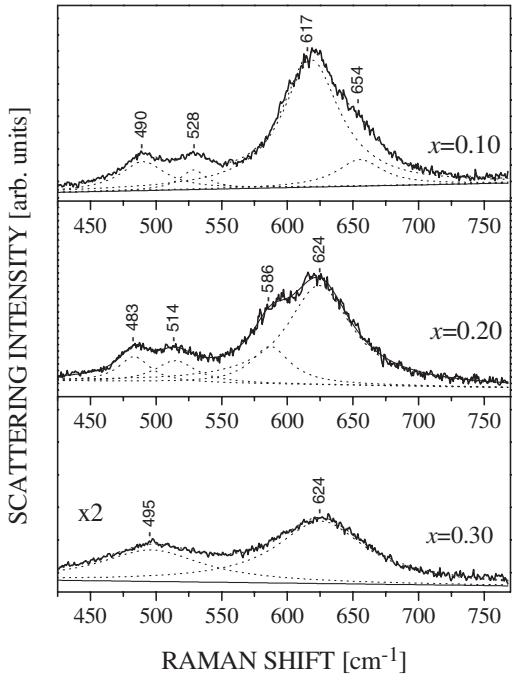

Figure 8. Evolution of the HV spectrum between $x = 0.10$ and 0.30.

line at 617 cm^{-1} correspond to the highest A_g and B_{2g} modes, respectively [10]. Therefore, the relatively weak band at 653–658 cm^{-1}, observed in the HH and HV spectra of $YMnO_3$, cannot be a proper Raman mode for the *Pnma* structure, but is rather due to contributions from zone-boundary phonons. This is consistent with lattice dynamical calculations, which predict for both $YMnO_3$ and $LaMnO_3$ the strongest PDOS peak close to this frequency [18]. This structure and another one near 490 cm^{-1}, where a PDOS maximum is also predicted, grow in relative weight with increasing x and become dominant at $x = 0.30$, while the lines related to Γ-point Raman modes, involving mainly oxygen motions, diminish. This is exactly what one expects upon loss of translation symmetry with increasing oxygen disorder. It is worth noting that the cationic sublattice also exhibits increasing disorder at higher x, indicated by noticeable broadening of the x-ray diffraction patterns for $x = 0.30$ and 0.50 (figure 1). The x-ray patterns gain their intensities mainly from the Y, Ca, and Mn atoms and to a lesser extent from the light oxygen atoms, which justifies such a conclusion.

4. Conclusions

We have successfully prepared orthorhombic $Y_{1-x}Ca_xMnO_3$ in a wide doping range between $x = 0$ and 0.5 using high-pressure synthesis. Between $x = 0$ and 0.25 the orthorhombic structure was stabilized as a metastable phase. The lattice parameters change gradually with x over the whole doping range. The Ca doping increases the conductivity, but its temperature dependence remains semiconducting for all x. The magnetic susceptibility for $x \leqslant 0.3$ exhibits the typical paramagnetic Curie dependence at high temperatures (>80 K). The paramagnetic Curie temperature is negative for small x, crosses zero at $x \approx 0.08$ and becomes positive at larger x. This is interpreted as a gradual change of the magnetic correlations from

antiferromagnetic superexchange ($x < 0.08$) to ferromagnetic double exchange interactions ($x > 0.08$) due to the replacement of Mn^{3+} with Mn^{4+} with increasing Ca doping. The evolution with x of the Raman spectra provides strong indications for increasing disorder of the oxygen sublattice for $x \geqslant 0.10$, presumably due to quasistatic and/or dynamic Jahn–Teller distortions. As a consequence of the loss of translational symmetry and the activation of otherwise forbidden vibrations, the relatively broad bands in the Raman spectra for high substitution levels reflect the phonon density of states rather than the Raman-allowed zone centre phonons.

Acknowledgments

This work is supported in part by the state of Texas through the Texas Center for Superconductivity and Advanced Materials, by NSF grant no DMR-9804325, the TLL Temple Foundation, the John J and Rebecca Moores Endowment, and at LBNL by the Director, Office of Science, Office of Basic Energy Sciences, Division of Materials Sciences and Engineering of the US Department of Energy under contract no DE-AC03-76SF00098.

References

[1] Moure C, Villegas M, Fernandez J F, Tartaj J and Duran P 1999 *J. Mater. Sci.* **34** 2565
[2] Waintal A and Chenavas J 1967 *C. R. Acad. Sci.* B **264** 168
[3] Coey J M D, Viret M and von Molnár S 1999 *Adv. Phys.* **48** 167 and references therein
[4] Brinks H W, Fjellvag H and Kjekshus A 1997 *J. Solid State Chem.* **129** 334
[5] Pollert E, Krupicka S and Kuzmicova E 1982 *J. Phys. Chem. Solids* **43** 1137
[6] Mathieu R, Nordblad P, Nam D N H, Phuc N X and Khiem N V 2001 *Phys. Rev.* B **63** 174405
[7] Laberty Ch, Navrotsky A, Rao C N R and Alphonse P 1999 *J. Solid State Chem.* **145** 77
[8] Munoz A, Alonso J A, Casais M T, Martinez-Lope M J, Martinez J L and Fernandez-Diaz M T 2002 *J. Phys.: Condens. Matter* **14** 3285
[9] Wood V E, Austin A E, Collings E W and Brog K C 1973 *J. Phys. Chem. Solids* **34** 859
[10] Iliev M N, Abrashev M V, Lee H-G, Popov V N, Sun Y Y, Thomsen C, Meng R L and Chu C W 1998 *Phys. Rev.* B **57** 2872
[11] Podobedov V B, Weber A, Romero D B, Rice J P and Drew H D 1998 *Solid State Commun.* **105** 589
Podobedov V B, Weber A, Romero D B, Rice J P and Drew H D 1998 *Phys. Rev.* B **58** 43
[12] Yoon S, Liu H L, Schollerer G, Cooper S L, Han P D, Payne D A, Cheong S-W and Fisk Z 1998 *Phys. Rev.* B **58** 2795
[13] Granado E, Moreno N O, Garcia A, Sanjurjo J A, Rettori C, Torriani I, Oseroff S B, Neumeier J J, McClellan K J, Cheong S-W and Tokura Y 1998 *Phys. Rev.* B **58** 11435
[14] Abrashev M V, Ivanov V G, Iliev M N, Chakalov R A, Chakalova R I and Thomsen C 1999 *Phys. Status Solidi* b **215** 631
[15] Liarokapis E, Leventouri Th, Lampakis D, Palles D, Neumeier J J and Goodwin D H 1999 *Phys. Rev.* B **60** 12758
[16] Björnsson P, Rübhausen M, Bäckström J, Käll M, Eriksson S, Eriksen J and Börjesson L 2000 *Phys. Rev.* B **61** 1193
[17] Iliev M N, Litvinchuk A P, Abrashev M V, Ivanov V G, Lee H-G, McCarrol W H, Greenblatt M, Meng R L and Chu C W 2000 *Physica* C **341–348** 2257
[18] Iliev M N, Abrashev M V, Popov V N and Hadjiev V G 2003 *Phys. Rev.* B **67** 212301